High-efficiency superconducting nanowire single-photon detectors fabricated from MoSi thin-films

Verma, V. B.; Korzh, Boris; Bussieres, Félix; Horansky, R. D.; Dyer, S. D.; Lita, A. E.; Vayshenker, I.; Marsili, F.; Shaw, M. D.; Zbinden, Hugo; Mirin, R. P.; Nam, S. W.

High-efficiency superconducting nanowire single-photon detectors fabricated from MoSi thin-films

V. B. Verma,[1,*] B. Korzh,[2] F. Bussières,[2] R. D. Horansky,[1] S. D. Dyer,[1] A. E. Lita,[1] I. Vayshenker,[1] F. Marsili,[3] M. D. Shaw,[3] H. Zbinden,[2] R. P. Mirin,[1] and S. W. Nam[1]

[1]*National Institute of Standards and Technology, 325 Broadway, Boulder, CO 80305, USA*
[2]*Group of Applied Physics, University of Geneva, CH-1211 Geneva 4, Switzerland*
[3]*Jet Propulsion Laboratory, California Institute of Technology, 4800 Oak Grove Dr., Pasadena, California 91109, USA*
[*]*verma@nist.gov*

Abstract: We report on MoSi SNSPDs which achieved high system detection efficiency (87.1 ± 0.5% at 1542 nm) at 0.7 K and we demonstrate that these detectors can also be operated with saturated internal efficiency at a temperature of 2.3 K in a Gifford-McMahon cryocooler. We measured a minimum system jitter of 76 ps, maximum count rate approaching 10 MHz, and polarization dependence as low as 3.3 ± 0.1%. The performance of MoSi SNSPDs at 2.3 K is similar to the performance of WSi SNSPDs at < 1 K. The higher operating temperature of MoSi SNSPDs makes these devices promising for widespread use due to the simpler and less expensive cryogenics required for their operation.

OCIS codes: (160.1890) Detector materials; (040.5570) Quantum detectors.

References and links

1. D. Rosenberg, A. J. Kerman, R. J. Molnar, and E. A. Dauler, "High-speed and high-efficiency superconducting nanowire single photon detector array," Opt. Express **21**(2), 1440–1447 (2013).
2. S. Miki, T. Yamashita, H. Terai, and Z. Wang, "High performance fiber-coupled NbTiN superconducting nanowire single photon detectors with Gifford-McMahon cryocooler," Opt. Express **21**(8), 10208–10214 (2013).
3. G. N. Goltsman, O. Okunev, G. Chulkova, A. Lipatov, A. Semenov, K. Smirnov, B. Voronov, A. Dzardanov, C. Williams, and R. Sobolewski, "Picosecond superconducting single-photon optical detector," Appl. Phys. Lett. **79**(6), 705 (2001).
4. C. M. Natarajan, M. G. Tanner, and R. H. Hadfield, "Superconducting nanowire single-photon detectors: physics and applications," Supercond. Sci. Technol. **25**(6), 063001 (2012).
5. F. Marsili, V. B. Verma, J. A. Stern, S. Harrington, A. E. Lita, T. Gerrits, I. Vayshenker, B. Baek, M. D. Shaw, R. P. Mirin, and S. W. Nam, "Detecting single infrared photons with 93% system efficiency," Nat. Photonics **7**(3), 210–214 (2013).
6. J. K. W. Yang and K. K. Berggren, "Using high-contrast salty development of hydrogen silsesquioxane for sub-10-nm half-pitch lithography," J. Vac. Sci. Technol. B **25**(6), 2025 (2007).
7. A. J. Kerman, E. A. Dauler, W. E. Keicher, J. K. W. Yang, K. K. Berggren, G. Gol'tsman, and B. Voronov, "Kinetic-inductance-limited reset time of superconducting nanowire photon counters," Appl. Phys. Lett. **88**(11), 111116 (2006).
8. B. S. Robinson, A. J. Kerman, E. A. Dauler, R. J. Barron, D. O. Caplan, M. L. Stevens, J. J. Carney, S. A. Hamilton, J. K. Yang, and K. K. Berggren, "781 Mbit/s photon-counting optical communications using a superconducting nanowire detector," Opt. Lett. **31**(4), 444–446 (2006).
9. F. Marsili, F. Najafi, E. Dauler, R. J. Molnar, and K. K. Berggren, "Afterpulsing and instability in superconducting nanowire avalanche photodetectors," Appl. Phys. Lett. **100**(11), 112601 (2012).
10. J. Zhang, W. Slysz, A. Verevkin, O. Okunev, G. Chulkova, A. Korneev, A. Lipatov, G. N. Gol'tsman, and R. Sobolewski, "Response time characterization of NbN superconducting single-photon detectors," IEEE Trans. Appl. Supercond. **13**(2), 180–183 (2003).
11. H. Takesue, S. W. Nam, Q. Zhang, R. H. Hadfield, T. Honjo, K. Tamaki, and Y. Yamamoto, "Quantum key distribution over a 40-dB channel loss using superconducting single-photon detectors," Nat. Photonics **1**(6), 343–348 (2007).

#252761 Received 28 Oct 2015; revised 9 Dec 2015; accepted 11 Dec 2015; published 22 Dec 2015

12. J. Chen, J. B. Altepeter, M. Medic, K. F. Lee, B. Gokden, R. H. Hadfield, S. W. Nam, and P. Kumar, "Demonstration of a quantum controlled-NOT gate in the telecommunications band," Phys. Rev. Lett. **100**(13), 133603 (2008).
13. C. Clausen, I. Usmani, F. Bussières, N. Sangouard, M. Afzelius, H. de Riedmatten, and N. Gisin, "Quantum storage of photonic entanglement in a crystal," Nature **469**(7331), 508–511 (2011).
14. M. J. Stevens, B. Baek, E. A. Dauler, A. J. Kerman, R. J. Molnar, S. A. Hamilton, K. K. Berggren, R. P. Mirin, and S. W. Nam, "High-order temporal coherences of chaotic and laser light," Opt. Express **18**(2), 1430–1437 (2010).
15. F. Bussières, C. Clausen, A. Tiranov, B. Korzh, V. B. Verma, S. W. Nam, F. Marsili, A. Ferrier, P. Goldner, H. Herrmann, C. Silberhorn, W. Sohler, M. Afzelius, and N. Gisin, "Quantum teleportation from a telecom-wavelength photon to a solid-state quantum memory," Nat. Photonics **8**(10), 775–778 (2014).
16. M. E. Grein, A. J. Kerman, E. A. Dauler, O. Shatrovoy, R. J. Molnar, D. Rosenberg, J. Yoon, C. E. DeVoe, D. V. Murphy, B. S. Robinson, and D. M. Boroson, "Design of a ground-based optical receiver for the lunar laser communications demonstration," 2011 Int. Conf. Sp. Opt. Syst. Appl. **78,** (2011).
17. G. Reithmaier, S. Lichtmannecker, T. Reichert, P. Hasch, K. Müller, M. Bichler, R. Gross, and J. J. Finley, "On-chip time resolved detection of quantum dot emission using integrated superconducting single photon detectors," Sci. Rep. **3**, 1901 (2013).
18. C. Zinoni, B. Alloing, L. H. Li, F. Marsili, A. Fiore, L. Lunghi, A. Gerardino, Y. B. Vakhtomin, K. V. Smirnov, and G. N. Gol'tsman, "Single photon experiments at telecom wavelengths using nanowire superconducting detectors," Appl. Phys. Lett. **91**(3), 031106 (2007).
19. A. McCarthy, N. J. Krichel, N. R. Gemmell, X. Ren, M. G. Tanner, S. N. Dorenbos, V. Zwiller, R. H. Hadfield, and G. S. Buller, "Kilometer-range, high resolution depth imaging via 1560 nm wavelength single-photon detection," Opt. Express **21**(7), 8904–8915 (2013).
20. M. G. Tanner, S. D. Dyer, B. Baek, R. H. Hadfield, and S. W. Nam, "High-resolution single-mode fiber-optic distributed Raman sensor for absolute temperature measurement using superconducting nanowire single-photon detectors," Appl. Phys. Lett. **99**(20), 201110 (2011).
21. J. Zhang, N. Boiadjieva, G. Chulkova, H. Deslandes, G. N. Gol'tsman, A. Korneev, P. Kouminov, M. Leibowitz, W. Lo, R. Malinsky, O. Okunev, A. Pearlman, W. Slysz, K. Smirnov, C. Tsao, A. Verevkin, B. Voronov, K. Wilsher, and R. Sobolewski, "Noninvasive CMOS circuit testing with NbN superconducting single-photon detectors," Electron. Lett. **39**(14), 1086 (2003).
22. V. B. Verma, F. Marsili, S. Harrington, A. E. Lita, R. P. Mirin, and S. W. Nam, "A three-dimensional, polarization-insensitive superconducting nanowire avalanche photodetector," Appl. Phys. Lett. **101**(25), 251114 (2012).
23. M. S. Allman, V. B. Verma, M. Stevens, T. Gerrits, R. D. Horansky, A. E. Lita, F. Marsili, A. Beyer, M. D. Shaw, D. Kumor, R. Mirin, and S. W. Nam, "A near-infrared 64-pixel superconducting nanowire single photon detector array with integrated multiplexed readout," Appl. Phys. Lett. **106**(19), 192601 (2015).
24. V. B. Verma, B. Korzh, F. Bussières, R. D. Horansky, A. E. Lita, F. Marsili, M. D. Shaw, H. Zbinden, R. P. Mirin, and S. W. Nam, "High-efficiency WSi superconducting nanowire single-photon detectors operating at 2.5 K," Appl. Phys. Lett. **105**(12), 122601 (2014).
25. V. B. Verma, A. E. Lita, M. R. Vissers, F. Marsili, D. P. Pappas, R. P. Mirin, and S. W. Nam, "Superconducting nanowire single photon detectors fabricated from an amorphous $Mo_{0.75}Ge_{0.25}$ thin film," Appl. Phys. Lett. **105**(2), 022602 (2014).
26. Y. P. Korneeva, M. Y. Mikhailov, Y. P. Pershin, N. N. Manova, A. V. Divochiy, Y. B. Vakhtomin, A. A. Korneev, K. V. Smirnov, A. G. Sivakov, A. Y. Devizenko, and G. N. Goltsman, "Superconducting single-photon detector made of MoSi film," Supercond. Sci. Technol. **27**(9), 095012 (2014).
27. A. J. Miller, A. E. Lita, B. Calkins, I. Vayshenker, S. M. Gruber, and S. W. Nam, "Compact cryogenic self-aligning fiber-to-detector coupling with losses below one percent," Opt. Express **19**(10), 9102–9110 (2011).
28. V. Anant, A. J. Kerman, E. A. Dauler, J. K. W. Yang, K. M. Rosfjord, and K. K. Berggren, "Optical properties of superconducting nanowire single-photon detectors," Opt. Express **16**(14), 10750–10761 (2008).
29. A. J. Kerman, D. Rosenberg, R. J. Molnar, and E. A. Dauler, "Readout of superconducting nanowire single-photon detectors at high count rates," J. Appl. Phys. **113**(14), 144511 (2013).
30. A. J. Kerman, J. K. W. Yang, R. J. Molnar, E. A. Dauler, and K. K. Berggren, "Electrothermal feedback in superconducting nanowire single-photon detectors," Phys. Rev. B **79**(10), 100509 (2009).

1. Introduction

Superconducting nanowire single-photon detectors (SNSPDs) have made rapid progress in recent years. To a large extent, this progress has resulted from materials research and development. Improvements in the deposition techniques for polycrystalline superconductors such as NbN and NbTiN SNSPDs have led to system detection efficiencies (SDE) above 70% at a wavelength of 1550 nm [1, 2], representing nearly an order of magnitude improvement over the first SNSPDs fabricated from NbN [3, 4]. Alternatively, SNSPDs based on the amorphous superconductor W_xSi_{1-x} have demonstrated ~93% SDE at 1550 nm [5]. In addition

#252761 Received 28 Oct 2015; revised 9 Dec 2015; accepted 11 Dec 2015; published 22 Dec 2015

to their high efficiencies, SNSPDs have also demonstrated fast recovery times (< 10 ns) [6–9], low jitter (< 100 ps) [10], and low intrinsic dark count rates (< 1 count per second, cps) [5]. SNSPDs are ideal detectors for demanding quantum optics experiments [11–15], as well as other applications such as long-distance ground-to-space optical communications [16], characterization of single-photon sources and photon pair sources [17, 18], light detection and ranging (LIDAR) [19], distributed fiber sensing [20], and integrated circuit testing [21].

Amorphous materials such as WSi are particularly desirable for the fabrication of SNSPDs due to their high degree of homogeneity and uniformity over large areas. Due to the lack of a well-defined crystal structure, amorphous superconductors can in principle be deposited on any smooth substrate (~1 nm RMS roughness) without significant degradation in material properties [22]. Thus, SNSPDs fabricated from these materials can easily be embedded inside of a dielectric optical stack to enhance absorption at a particular wavelength. Amorphous materials have also led to innovations in device design including multilayer polarization-independent nanowire detectors [22] and SNSPD arrays [23].

One characteristic feature of WSi SNSPDs is their detection efficiency that can be saturated at telecommunications wavelengths (λ = 1550 nm) with wider nanowires (~150 nm) than with NbN devices (~30 nm). This effect, which is likely due to the lower superconducting gap energy and lower carrier density of WSi, reduces the constraints on the precision of the nanofabrication process. Also, operating into the plateau region is a practical advantage that provides stability against small temperature and bias current fluctuations. The operating temperature also has a practical importance. A saturated efficiency as high as 78% at 1310 nm and 2.5 K was reported with WSi [24]. However, when this WSi device was characterized at 1550 nm, the beginning of the efficiency plateau moved beyond its switching current (the current at which the device switches from the superconducting to the normal state), and the efficiency no longer saturated.

The switching current in WSi is also lower than typical NbN and NbTiN values, which increases the jitter to ~150-200 ps [5, 24]. The hope of obtaining better performance instigated research into other amorphous superconductors with slightly higher T_C, such as MoGe [25] and MoSi [26]. However, the efficiencies reported with these materials have so far been well below 80%, which is due to the lack of an optical cavity designed to enhance absorption [5, 25, 26]. Finally, a saturated efficiency at 1550 nm at ~2.5 K has not been demonstrated with amorphous superconductors. Achieving a large and saturated efficiency at higher temperatures is important; it would relax the requirements on the cryogenic system and simplify their integration in complex experiments requiring the most demanding performance.

Here we report on the performance of MoSi SNSPDs embedded inside of an optical stack designed to enhance absorption at a wavelength of 1550 nm. We demonstrate an efficiency of 87.1 ± 0.5% at 1542 nm and a temperature of 0.7 K, approaching the best efficiency achieved to date with WSi-based devices (93% at 1550 nm) [5], with significantly lower jitter (76 ps at 0.7 K) than WSi (~150 ps at 0.12 K) [5]. We also demonstrate a saturated efficiency of 82% at 1550 nm at 2.5 K.

2. Experiment

The fabrication process begins with the deposition of gold mirrors on a 3 inch Si wafer by electron beam evaporation and liftoff. The mirrors consist of 80 nm of Au with a 2 nm Ti adhesion layer below and above the mirror. A quarter-wave spacer layer consisting of 235 nm of SiO_2 is then deposited by plasma-enhanced chemical vapor deposition (PECVD), and Ti/Au contact pads are patterned by liftoff. The 6.6 nm-thick MoSi film is deposited by DC magnetron sputtering from an alloy target with a composition of 75:25 atomic percent Mo:Si at room temperature and capped with 2 nm of amorphous Si to prevent oxidation. The composition of the sputtered film may differ from the composition of the target. However, we did not perform composition measurements of the film after deposition. The thickness of the αSi layer was estimated based on the deposition of a thick film, patterning, etching, and

#252761 Received 28 Oct 2015; revised 9 Dec 2015; accepted 11 Dec 2015; published 22 Dec 2015

measurement of the thickness with an atomic force microscope (AFM). To estimate the thickness of the MoSi, we measured the thickness of the etched SNSPD using an AFM, and subtracted the 2 nm thickness of the αSi cap. The etch rate of the material was carefully calibrated in order to minimize etching into the SiO_2 substrate, but we note that any overetch into the underlying SiO_2 may result in a slight overestimate of the thickness. The optical constants of the film measured at a wavelength of 1550 nm are n = 4.7 and k = 2.9.

After etching a 20 µm-wide strip between the gold contact pads, electron beam lithography and etching in an SF_6 plasma are used to define the nanowire meanders. An antireflection coating is deposited on the top surface consisting of 294 nm SiO_2, 234 nm SiN_x, 169 nm SiO_2, and 161 nm SiN_x. A keyhole shape is then etched through the Si wafer around each SNSPD, which can then be removed from the wafer and self-aligned to a single-mode optical fiber to within ± 3 µm [27]. Each nanowire meander covers an active area of 16 µm × 16 µm which is larger than the 10 µm mode-field diameter of a standard single-mode fiber to allow for misalignment.

We characterized two SNSPDs from the same fabrication run. One SNSPD was characterized at a temperature of 0.7 K using a water-cooled closed-cycle cryocooler augmented by a ^{4}He sorption pump unit, while the other was characterized in an air-cooled Gifford-McMahon cryocooler with 100 mW of cooling power operating at 2.3 K.

A 1542 nm CW laser attenuated to a mean photon number of ~300,000 photons/s was used for the measurements at 0.7 K. The calibration of the input power to the SNSPD was performed as outlined in [3] using a NIST-calibrated InGaAs power meter. Although the detector was optimized for a wavelength of 1550 nm, measurements were performed at 1542 nm because the power meter was calibrated at that wavelength. The absorption efficiency at 1542 nm was modelled to be 98.7%, only 0.4% lower than the maximum at 1550 nm. Figure 1 shows the system detection efficiency (SDE) and background count rate (BCR) as a function of bias current (I_B) normalized to the switching current (I_{SW} = 9.5 µA, the bias current at which the device switches from the superconducting to the normal state) for a nanowire with a nominal width of 130 nm and pitch (center-to-center spacing between nanowires in the meander) of 215 nm. We define SDE as the probability that a photon in the optical fiber generates an electrical pulse from the detector. BCR is defined as the detector count rate

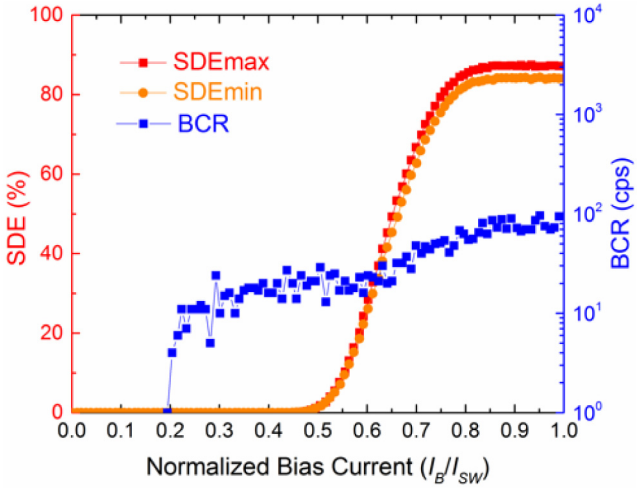

Fig. 1. System detection efficiency (SDE) and background count rate (BCR) as a function of normalized bias current. The switching current of the detector (I_{SW}) was 9.5 uA.

measured with the input port of the fiber to the cryostat blocked.

#252761 Received 28 Oct 2015; revised 9 Dec 2015; accepted 11 Dec 2015; published 22 Dec 2015

The SDE was measured after both maximizing (SDE_{max}) and minimizing (SDE_{min}) the detector counts as a function of the polarization of the incident light. The maximum and minimum SDE were determined from a 6-state Stokes measurement of count rates from the detector. At I_B ~0.95I_{SW}, the maximum SDE (SDE_{max}) was 87.1 ± 0.5% and the minimum SDE (SDE_{min}) was 84.3 ± 0.4% with a BCR of ~100 cps. Note the low polarization ratio (defined as SDE_{max}/SDE_{min}) of only 3.3 ± 0.1%, which we attribute to the high fill factor of the device and careful design and simulation of the optical stack. The polarization dependence is significantly lower than most results reported to date with both NbN [28] and WSi-based [5] SNSPDs. The low polarization dependence could in principle also be obtained with WSi through optimization of the fill factor, dielectric materials used in the optical stack, and layer thicknesses. The BCR was reduced by coiling the optical fiber close to the detector in order to increase the loss for long-wavelength blackbody radiation which is the dominant contribution to the BCR well below the switching current. The fiber was coiled 5.5 times with a 35 mm diameter. Loss due to the coil was measured to be ~0.1 dB.

The optical stack for these SNSPDs was designed for maximum absorption (99.1%) at a wavelength of 1550 nm. In addition to loss introduced by the fiber coil, discrepancy between the simulated absorption and measured SDE could be attributed to a number of factors including imperfect knowledge of the optical constants and thicknesses of the materials in the optical stack, small changes in the optical constants of the materials between room temperature and cryogenic temperatures, and an intrinsic quantum efficiency (the probability of converting absorbed photons into output pulses) which is less than unity. Misalignment between fiber and detector could also contribute to the loss. Although the mode field diameter of the fiber is 10.4 ± 0.8 μm which is smaller than the 16 μm size of the detector area, a 3 μm misalignment (the maximum expected based on previous measurements of alignment accuracy) could result in a reduction in coupling efficiency because a small fraction of the mode extends outside of the mode field diameter. Further research is required in order to

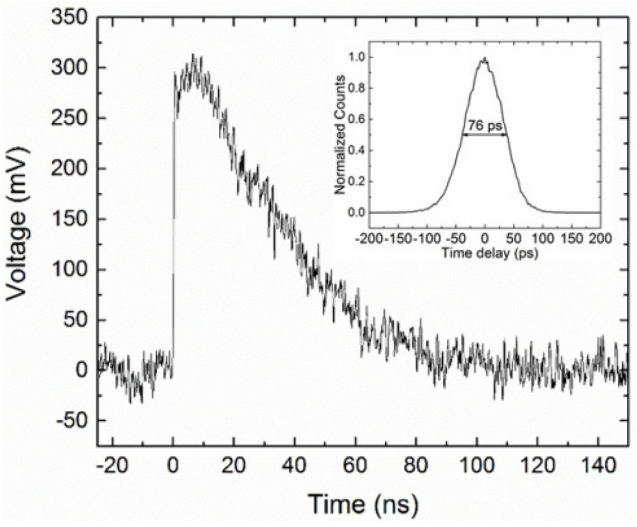

Fig. 2. Voltage pulse from the SNSPD obtained using two room temperature amplifiers with 51 dB total gain. Inset shows the instrument response function (IRF) of the detector system. The jitter, defined as the full width at half maximum (FWHM) of the IRF, is 76 ps.

understand the dominant contribution to the discrepancy between experiment and theory.

Figure 2 shows an output pulse from the SNSPD obtained using a chain of a 500 MHz amplifier with 28 dB of gain followed by a 1 GHz amplifier with 23 dB of gain, both operated at room temperature. The rise time of the pulse is 1 ns, and the 1/*e* decay time 35 ns. From this value of the decay time and the geometry of the nanowire, we extract a kinetic inductance

#252761 Received 28 Oct 2015; revised 9 Dec 2015; accepted 11 Dec 2015; published 22 Dec 2015

of 190 pH/square for the 6.6 nm-thick MoSi film. This value is somewhat lower than that reported for typical WSi films, which can range between 250 and 350 pH/square depending on the composition and thickness of the film. The jitter of the detector system (J_S), defined as the full width at half maximum (FWHM) of the instrument response function (IRF) of the detector system, was measured using a 1550 nm picosecond pulsed laser and 1 GHz oscilloscope to register the inter-arrival time between the laser pulse and the SNSPD pulse. The inset to Fig. 2 shows the IRF of the detector system biased at $I_B = 0.95I_{SW}$, which is the bias current corresponding to maximum SDE and a BCR of ~100 cps. The FWHM of the IRF yields $J_S = 76$ ps.

As shown in Fig. 2, the pulse height is ~300 mV, which is a factor of 2 larger than our measurements of the pulse height of WSi SNSPDs (~150 mV pulse height using identical amplifiers), which is the result of the factor of 2 higher I_{SW} in this MoSi SNSPD compared to a typical WSi SNSPD [5]. The larger pulse height results in a higher signal-to-noise ratio. The rise times of the pulses from both the MoSi and typical WSi SNSPDs are ~1 ns, thus the system jitter is reduced by the increase in signal-to-noise ratio, also by a factor of 2.

Measurements were also performed in a different cryogenic system operating at 2.3 K and with a narrower nanowire device (110 nm with a pitch of 185 nm). The cryogenic system is an air-cooled Gifford-McMahon cryocooler with 100 mW of cooling power. Figure 3 shows the SDE and BCR as a function of I_B normalized to the switching current $I_{SW} = 4.34$ μA. Measurements were performed with a CW 1550 nm laser with a photon flux of ~100,000 photons/s.

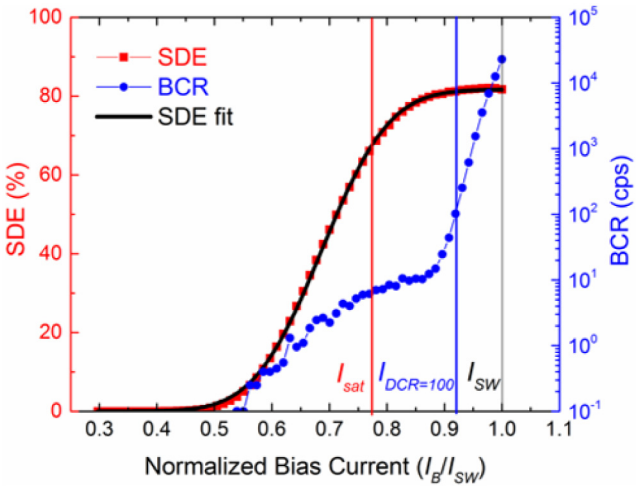

Fig. 3. System detection efficiency (SDE) and background count rate (BCR) as a function of normalized bias current for a 110 nm-wide nanowire operated at 2.3 K. The switching current of the detector (I_{SW}) was 4.34 uA.

The switching current is lower than the device described above ($I_{SW} = 9.5$ μA) due to the narrower nanowire combined with a higher operating temperature. Maximum SDE for this device is 82 ± 2% with the polarization optimized to maximize the count rate. The polarization ratio of this device is 10.3 ± 0.4% at 1550 nm, and 8.9 ± 0.6% at 1542 nm. The transmission of the fiber was measured to be 97.8%. Thus, an additional 2.2% in SDE could be gained by eliminating the fiber loss, which was most likely caused by an imperfect fiber splice. The lower SDE measured on this 110 nm-wide nanowire device compared to the 130 nm device can be attributed to the change in the SNSPD meander geometry (changes in width, pitch, and fill factor). When an optical cavity is designed, it is optimized for a particular meander geometry. Changes in the geometry relative to the optimum design result in corresponding changes in the absorption efficiency of the SNSPD. In this case, the cavity

#252761 Received 28 Oct 2015; revised 9 Dec 2015; accepted 11 Dec 2015; published 22 Dec 2015

was optimized for a 130 nm-wide nanowire with a pitch of 200 nm. Thus the device from Fig. 1 is much closer to the optimized geometry compared to the device from Fig. 3. The higher polarization ratio for the 110 nm-wide nanowire can also be attributed to a narrower wire geometry [28] and non-optimal cavity design for this specific width and pitch.

Despite the increased temperature, we observed saturation of the internal efficiency similar to lower temperatures. The BCR was below 10 cps for $I_B < 0.9I_{SW}$. The SDE was 81.2% for a BCR = 100. A coil was also used in this measurement to reduce background counts due to blackbody photons in the fiber.

To better quantify how the performance of the detector varies with the operating temperature, we cooled the same device presented in Fig. 3 (110 nm with a pitch of 185 nm) using a ^{4}He sorption cryocooler. We obtained curves like the ones presented in Fig. 3 for temperatures ranging from 0.8 to 2.6 K. The immediate consequences of cooling the device is that both the bias current I_B at which the plateau is reached and the switching current I_{SW} become larger with decreasing temperatures. However, the switching current increases faster, resulting in a plateau that becomes longer. The dark count rate also decreases for a given value of I_B. Hence, a lower temperature allows operating deeper into the plateau for a given dark count value. From this behavior, we can determine the maximum operating temperature for which we can get both a quasi-saturated efficiency at a user-determined dark count rate. To determine this temperature, we first fit the efficiency curves with an offset error function,

$$\frac{\eta_{\max}}{2}\left(1+\frac{erf\left(I_B-I_0\right)}{w}\right) \tag{1}$$

where η_{max} is the maximum efficiency, I_B is the bias current, I_0 is the offset of the error function and w is the fitting parameter corresponding to the width of the function. We define the saturation current, I_{SAT}, as the current at which the efficiency reaches 80% of η_{max}. We then find the current at which the dark count rate reaches 100 cps ($I_{DCR = 100}$). The switching current is the point at which the detector ceases to detect photons, either due to the surpassing of the critical current or detector latching. These three characteristic currents are identified in Fig. 3, and Fig. 4 shows how they vary with temperature. With our choice of $I_{DCR = 100}$, the maximum temperature at which this detector can be operated in the quasi-saturated regime is ~2.4 K. Tolerating a high dark count rate allows operating until 2.6 K, where the switching current reaches the saturation current and the plateau disappears. As can be seen from Fig. 3, at $I_{DCR = 100}$, the dark counts have an exponential dependence on the bias current, which means that they are dominated by the intrinsic dark counts of the device, not the blackbody radiation which is dominant below about $0.9I_{SW}$. This was observed for all of the measurements between 0.8 K and 2.6 K with this device.

Note, however, that such exponential behavior of the BCR in not seen in Fig. 1 and we

#252761 Received 28 Oct 2015; revised 9 Dec 2015; accepted 11 Dec 2015; published 22 Dec 2015

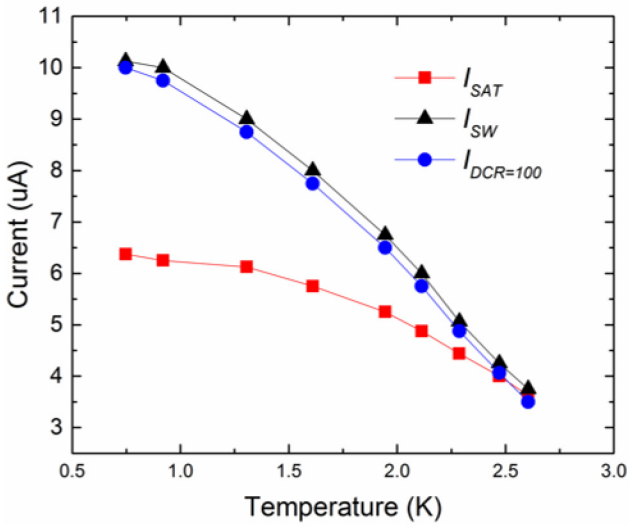

Fig. 4. Characteristic currents I_{SAT}, I_{SW}, and $I_{DCR\,=\,100}$ as a function of temperature.

believe that this is due to the fact that in this case the SNSPD was AC coupled to the readout electronics. As discussed in [29], the use of an AC-coupled readout can result in the reduction of the latching current (I_{latch}), where the detector switches into the normal state due to stable electrothermal feedback [30]. If I_{latch} is below the critical current, then it is no longer possible to operate the detector at high bias currents where the DCR behavior becomes exponential. The data presented in Figs. 3 and 4 was measured with a DC-coupled cryogenic amplifier (described below) which avoids this reduction of I_{latch}. We believe that using DC-coupled amplifiers for the detector presented in Fig. 1 would result in an increased I_{SW}, leading to a longer plateau and an exponential behavior of the DCR as is common close to the critical current.

At an operating temperature of 2.3 K, achieved with the Gifford-McMahon cryocooler, the bias current is inevitably reduced compared to lower temperatures. This means that the electrical signal-to-noise ratio of the readout signal decreases, increasing the system jitter. In order to improve the signal-to-noise ratio, reduce jitter, and obtain the maximum possible count rate from the detector, a DC-coupled cryogenic preamplifier was installed at the 40 K stage of the Gifford-McMahon cryocooler with 28 dB of gain, a bandwidth of 1 GHz, and a noise figure of 1.5 dB at 1575 MHz. The resulting signal was further amplified by a room-temperature amplifier with 33 dB of gain and bandwidth of 1 GHz. A 600 MHz filter was used following the output of the room-temperature amplifier to reduce noise on the output pulse. Figure 5 shows a voltage pulse from the SNSPD. The jitter of the detector system was measured using a 1550 nm pulsed laser with a FWHM of ~33 ps and a time-correlated single-photon counting card to register the inter-arrival time between the laser pulse and SNSPD pulse. The inset to Fig. 5 shows the IRF of the detector system biased at $I_B = 0.95I_{SW}$, which is the bias current corresponding to an SDE of 82% and a BCR of ~1500 cps. The system jitter is J_S = 99 ps. Figure 6 shows the system jitter as a function of normalized bias current. The system jitter decreases with increasing bias current due to the larger pulse amplitude and higher signal-to-noise ratio at higher bias currents. Figure 7 shows a plot of the count rate as a function of the input photon flux. The count rate remains linear up to photon fluxes approaching 10^7 photons/s.

We note that we did not measure the SDE of this particular device with both AC- and DC-coupled readout electronics, and thus cannot compare the efficiency measured with both readout techniques. As explained previously, the use of an AC-coupled readout can result in a slightly lower I_{SW}. As long as the efficiency near the AC-coupled I_{SW} is in the plateau region

#252761 Received 28 Oct 2015; revised 9 Dec 2015; accepted 11 Dec 2015; published 22 Dec 2015

of the curve, one would not expect a change in efficiency. However, if the AC-coupled I_{SW} falls below the plateau region, the SDE could be lower. The effect of different readout techniques on the SDE is beyond the scope of this paper, and is a subject for further investigation.

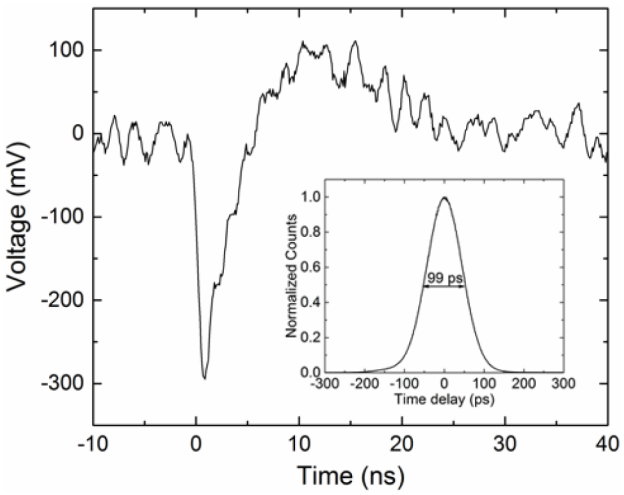

Fig. 5. Voltage pulse from the 110 nm-wide SNSPD at 2.3 K obtained using a cryogenic amplifier at 40 K and a room temperature amplifier. Inset shows the instrument response function (IRF) of the detector system. The system jitter is 99 ps.

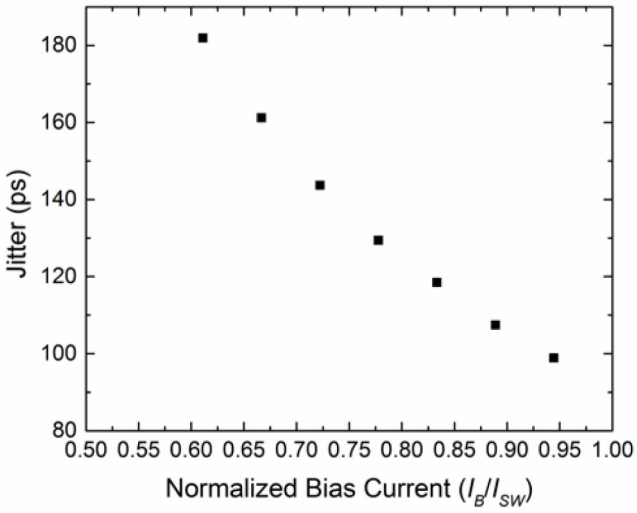

Fig. 6. Experimentally measured system jitter as a function of normalized bias current.

#252761 Received 28 Oct 2015; revised 9 Dec 2015; accepted 11 Dec 2015; published 22 Dec 2015

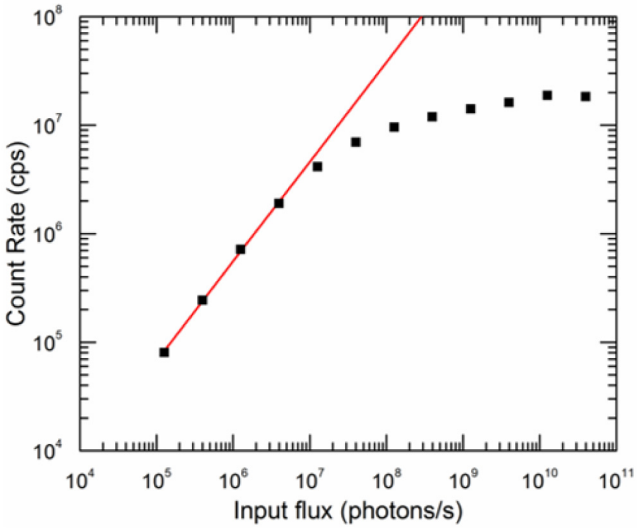

Fig. 7. Measured count rate as a function of the input photon flux (black squares). The red solid line is a linear fit to the first four data points.

3. Conclusion

We have demonstrated high-efficiency MoSi SNSPDs embedded in a dielectric stack to enhance absorption. The SNSPDs show a saturated internal efficiency as high as 87.1 ± 0.5% at a wavelength of 1542 nm with dark count rates below 100 cps. The lowest measured jitter was 76 ps at a temperature of 0.7 K. We demonstrated that even at a temperature of 2.3 K the MoSi SNSPDs exhibit high saturated internal efficiency. The devices remain linear in count rate with input photon fluxes approaching 10^7 photons/s, and show a low polarization dependence of only 2.8%. Our results indicate that MoSi SNSPDs operating at 2.3 K achieve the same performance as WSi SNSPDs at < 1 K. Since cryogenics is less complex and costly at 2.3 K than at < 1 K, MoSi SNSPDs have great potential for widespread use. We note that although MoSi SNSPDs appear to offer better performance than WSi at 2.3 K, our results do not preclude the possibility that similar performance could be obtained through further optimization of the WSi film thickness, composition, and nanowire geometry. However, the higher bulk transition temperature of MoSi compared to WSi suggests that MoSi may be a more desirable material for operation at 2.3 - 2.5 K, and our results support this hypothesis. Finally, the yield of MoSi devices so far appears to be similar to that of WSi devices, implying that MoSi may be a good material for the further development of SNSPD arrays. However, more MoSi SNSPDs must be tested in order to compare the yields more quantitatively.

Acknowledgments

We acknowledge Claudio Barreiro for useful discussions, and the Swiss Federal Institute of Metrology (METAS) for the calibration of the power meters. NIST funding provided by the DARPA InPho and QUINESS programs. Part of the work was funded by the Swiss NCCR Quantum Science in Technology project.

#252761 Received 28 Oct 2015; revised 9 Dec 2015; accepted 11 Dec 2015; published 22 Dec 2015